

Velocity-Density Correlations from the *cosmicflows-3* Distance Catalog and the 2MASS Redshift Survey

Adi Nusser^{*} †

14 October 2018

ABSTRACT

The peculiar velocity of a mass tracer is on average aligned with the dipole modulation of the surrounding mass density field. We present a first measurement of the correlation between radial peculiar velocities of objects in the *cosmicflows-3* catalog and the dipole moment of the 2MRS galaxy distribution in concentric spherical shells centered on these objects. Limiting the analysis to *cosmicflows-3* objects with distances of $100h^{-1}$ Mpc, the correlation function is detected at a confidence level $\gtrsim 4\sigma$. The measurement is found consistent with the standard Λ CDM model at $\lesssim 1.7\sigma$ level. We formally derive the constraints $0.32 < \Omega^{0.55}\sigma_8 < 0.48$ (68% confidence level) or equivalently $0.34 < \Omega^{0.55}/b < 0.52$, where b is the galaxy bias factor. Deeper and improved peculiar velocity catalogs will substantially reduce the uncertainties, allowing tighter constraints from this type of correlations.

Key words: dark matter – large-scale structure of Universe

1 INTRODUCTION

The peculiar velocity of a galaxy is expected to be correlated with its surrounding matter distribution. A classic example is the motion of the Local Group (LG) of galaxies relative to the frame of reference defined by the temperature anisotropy of the cosmic microwave background (CMB). The dipole component of the CMB temperature implies a motion of $V_{lg} = 627 \pm 22 \text{ km s}^{-1}$ in the direction $(l, b) = (276^\circ \pm 3^\circ, 30^\circ \pm 3^\circ)$ (e.g. Kogut et al. 1993). In accordance with gravitational instability theory for structure formation (Peebles 1980), this motion is produced by the cumulative gravitational pull of the observed large scale structure as probed by a variety of surveys of the galaxy distribution (e.g. Strauss & Davis 1988; Lynden-Bell et al. 1989; Schmoldt et al. 1999; Cieliegiak & Chodorowski 2004; Bilicki et al. 2011; Carrick et al. 2015). Any deviations can easily be explained within the limitations of current surveys (Nusser et al. 2014). More generally, the analysis of Davis et al. (2011) demonstrated a tight correlation between the observed radial velocities of galaxies in the SFI++ (Springob et al. 2007) catalog and the gravitational force field corresponding to the galaxy distribution in the $K_s \leq 11.25$ Two Mass Galaxy Redshift survey (2MRS) (Huchra et al. 2012).

The analyses above required a derivation of the gravitational field from a given distribution of galaxies in a redshift survey. In the case of the radial peculiar velocity versus

gravity comparison, equivalent smoothing of the two fields is also essential. Here we aim at a simpler approach which can be implemented more directly, alleviating the complex steps in the analysis above. We aim at a direct measurement of the $u - \delta$ correlation between radial motion, u , of galaxies and the dipole moment of the density contrast, δ , on spherical shells centered on the galaxies. We will perform the correlation using the radial peculiar velocities from the *cosmicflows-3* catalog (Tully et al. 2016) and the galaxy distribution in the $K_s \leq 11.75$ 2MRS. These two data sets match in depth and are the best available in terms of sky coverage.

This $u - \delta$ correlation greatly mitigates several complications inherently present in the more detailed velocity-gravity comparison. As we shall see, by taking the dipole moment of the correlation function, the “Kaiser rocket” effect (Kaiser 1988) resulting from the flux limit nature of the redshift survey is essentially eliminated. The estimation of the correlation does not require any smoothing of either the peculiar velocity data or the galaxy distribution.

The outline of the paper is as follows. In §2 we provide definitions for the basic quantities. The theoretical framework and predictions in the Λ CDM model are presented in §3. The main properties of the observational data, *cosmicflows-3* and 2MRS, are briefly described in §4. This section also gives details of how the correlations are estimated from the observations. Errors associated with the observed correlations will be assessed using mock galaxy catalogs as described in §5. The results of $u - \delta$ correlations and implications on cosmological parameters follow in §6. In §6.3

^{*} adi@physics.technion.ac.il

[†] Physics Department and the Asher Space Science Institute-Technion, Haifa 32000, Israel

we provide a preliminary assessment of 3D velocity density correlations. We conclude with a general discussion in §7.

Our notation is as follows. The expansion parameter is a and is related to the redshift z by $a = (1+z)^{-1}$. The Hubble function is $H(t) = \dot{a}/a$ and is denoted by H_0 at the present epoch. We adopt the Λ CDM cosmological model denoting by Ω and Λ the mass energy density parameters in units of the critical density. The growth factor of linear density perturbations is $D(t)$ and the growth rate is $f(z) = d \ln D / d \ln a$. The growth rate mainly depends on the mass density parameter $\Omega(z)$ and is well approximated by $f \approx \Omega^{0.55}$ in a Λ CDM cosmology (Linder 2005). Further, we define the correlation function $\xi_{fg} \equiv \langle f(\mathbf{r})g(\tilde{\mathbf{r}}) \rangle$ between any two fields f and g at points \mathbf{r} and $\tilde{\mathbf{r}}$ as the ensemble average over many random realizations of the fields.

2 BASICS

The density contrast is defined as $\delta(\mathbf{r}) = \rho(\mathbf{r})/\bar{\rho} - 1$, where $\bar{\rho}$ is the mean background density. The comoving coordinate of a patch of matter is \mathbf{r} and the corresponding comoving peculiar velocity is \mathbf{v} (physical is $a\mathbf{v}$). Linear theory of cosmological gravitational instability (Peebles 1980) relates \mathbf{v} and δ via

$$\delta(\mathbf{r}) = -\frac{1}{f} \nabla \cdot \mathbf{v}(\mathbf{r}), \quad (1)$$

where distance coordinates are expressed in km s^{-1} . This, however, is the real density contrast corresponding to mass per unit volume $d^3r = r^2 dr d\Omega$ in actual distance space. Surveys of the galaxy distribution provide redshifts, cz (in km s^{-1}), of galaxies rather than distances. The latter are provided in distance indicator catalogs for a smaller set of galaxies. The observed redshifts are given in terms of the comoving distance, r , and the radial component $u = \mathbf{v} \cdot \hat{\mathbf{r}}$ of \mathbf{v} (Sachs & Wolfe 1967),

$$cz = cz_c + u \quad (2)$$

where z_c is the cosmological redshift calculated from the actual comoving distance¹, r , of the galaxy and, since we are considering low redshift data only, we have neglected gravitational contributions. By continuity and to linear order, density contrast of matter in redshift space, δ^s , differs from δ by the divergence of the displacement. Therefore,

$$\delta^s = \delta - \nabla \cdot (u\hat{\mathbf{r}}). \quad (3)$$

We write

$$\nabla \cdot (u\hat{\mathbf{r}}) = \hat{r}_i \hat{r}_j \frac{\partial v_i}{\partial x_j} + \frac{2u}{r}, \quad (4)$$

where \hat{r}_i is cosine the angle between $\hat{\mathbf{r}}$ and the cartesian axis defined by the unit vector $\hat{\mathbf{x}}_i$ and summation over repeated indices is implied. The derivatives and all other quantities are taken as a function of the real space coordinate r which, to linear order, are equivalent to quantities expressed in terms of coordinates in redshift space.

Therefore, observational data of radial peculiar motions

¹ If r_{Mpc} is the comoving distance in Mpc then $dr = H dr_{\text{Mpc}} = cdz_c$

and the distribution of galaxies in redshift space allow a direct estimation of the correlation function

$$\xi_{u\delta}^s = \langle u(\mathbf{r})\delta^s(\tilde{\mathbf{r}}) \rangle. \quad (5)$$

rather than $\xi_{u\delta} = \langle u(\mathbf{r})\delta(\tilde{\mathbf{r}}) \rangle$ between u and the real space density field, δ . The superscript s on ξ will be reserved for velocity-density correlation in redshift space.

The relation (3) implies

$$\xi_{u\delta}^s = \xi_{u\delta} + \xi_{uw} - \frac{2\xi_{uu}}{\tilde{r}}, \quad (6)$$

where $w = -\hat{r}_i \hat{r}_j \partial v_i / \partial \tilde{x}_j$. We begin with a theoretical description of $\xi_{u\delta}^s$ in linear theory and then we proceed to compute these correlations from mock and real data.

3 THEORETICAL CORRELATIONS

Expressions for each of the terms on the r.h.s of (6) can be conveniently derived using the formalism developed by Gorski (1988) for describing velocity correlations. The correlation of the cartesian components v_i and v_j at different points in space is

$$\xi_{v_i v_j} = \Psi_{\perp}(y)\delta_{ij}^K + [\Psi_{\parallel}(y) - \Psi_{\perp}(y)]\hat{y}_i \hat{y}_j, \quad (7)$$

where δ_{ij}^K is Kronecker's delta function. The ‘‘perpendicular’’ and ‘‘parallel’’ (to the separation $\mathbf{y} = \tilde{\mathbf{r}} - \mathbf{r}$) correlation functions Ψ_{\perp} and Ψ_{\parallel} are given in terms of the density power spectrum, $P(k)$, as

$$\Psi_{\perp, \parallel}(y) = \frac{f^2}{2\pi^2} \int_0^{\infty} P(k) K_{\perp, \parallel}(ky) dk, \quad (8)$$

where $K_{\perp}(x) = j_1(x)/x$ and $K_{\parallel}(x) = j_0(x) - 2j_1(x)/x$ and $j_l(x)$ are spherical Bessel functions of order l .

For $\xi_{uu} = \langle \hat{r}_i v_i(\mathbf{r}) \hat{r}_j v_j(\tilde{\mathbf{r}}) \rangle$, the relation (7) yields

$$\xi_{uu} = \nu \Psi_{\perp} + \mu \tilde{\mu} \Psi_{-}, \quad (9)$$

where $\Psi_{-} = \Psi_{\parallel} - \Psi_{\perp}$, $\mu = \hat{\mathbf{r}} \cdot \hat{\mathbf{y}}$, $\tilde{\mu} = \hat{\tilde{\mathbf{r}}} \cdot \hat{\mathbf{y}}$ and $\nu = \hat{\mathbf{r}} \cdot \hat{\tilde{\mathbf{r}}}$. To derive ξ_{uw} , we write²

$$\begin{aligned} \left\langle \frac{\partial v_i}{\partial \tilde{x}_j} v_m \right\rangle &= \Psi'_{\perp} \hat{y}_j \delta_{im}^K + \Psi'_{-} \hat{y}_i \hat{y}_j \hat{y}_m \\ &+ \frac{\Psi_{-}}{y} \left(\delta_{ij}^K \hat{y}_m + \delta_{jm}^K \hat{y}_i \right) - 2 \frac{\Psi_{-}}{y} \hat{y}_i \hat{y}_j \hat{y}_m. \end{aligned} \quad (10)$$

where primes denote derivatives with respect to y . Therefore, contracting with $\hat{r}_i \hat{r}_j$ gives

$$\xi_{uw} = -[\Psi'_{\perp}(2\tilde{\mu}\nu + \mu) + (\Psi'_{-} - 2\Psi'_{\perp})\tilde{\mu}^2\mu]. \quad (11)$$

According to the linear relation (1), the correlation of u with real space density is $\xi_{u\delta} = -\xi_{\theta u}/f$ where $\theta = \nabla \cdot \mathbf{v} = \delta_{ij}^K \frac{\partial v_i}{\partial \tilde{x}_j}$. From (7) we have,

$$\xi_{\theta\theta} = (3\Psi'_{\perp} + \Psi'_{-})\hat{\mathbf{y}}, \quad (12)$$

where we have used $\Psi_{-} = y\Psi'_{\perp}$ (Gorski 1988). Thus, $\xi_{u\theta} = \langle u(\mathbf{r})\theta(\tilde{\mathbf{r}}) \rangle = \hat{\mathbf{r}} \cdot \xi_{\theta\theta}$ and hence

$$\xi_{u\delta} = -\frac{1}{f} (3\Psi'_{\perp} + \Psi'_{-})\mu. \quad (13)$$

² $\partial y / \partial \tilde{x}_i = \hat{y}_i$ and $\partial \hat{y}_i / \partial \tilde{x}_j = \delta_{ij}^K / y = \hat{y}_i \hat{y}_j / y$ where $y = \sqrt{\sum_i (\tilde{x}_i - x_i)^2}$.

For later use we also list

$$\xi_{uv_j} = \langle \hat{r}_i v_i(\mathbf{r}) v_j(\tilde{\mathbf{r}}) \rangle = \Psi_{\perp} \hat{r}_j + \mu \Psi_{-} \hat{y}_j. \quad (14)$$

Collecting all terms, we arrive at

$$\begin{aligned} \xi_{u\delta}^s(\mathbf{r}, \tilde{\mathbf{r}}) &= -\frac{1}{f} (3\Psi'_{\perp} + \Psi'_{-}) \mu \\ &- 3\Psi'_{\perp} \mu - \Psi'_{\perp} (2\tilde{\mu} \nu + \mu) - (\Psi'_{-} - 2\Psi'_{\perp}) \tilde{\mu}^2 \mu \\ &- \frac{2\nu\Psi_{\perp} + \mu\tilde{\mu}\Psi_{-}}{\tilde{r}}, \end{aligned} \quad (15)$$

where ν and $\tilde{\mu}$ are expressed in terms of y , r and μ .

The form of the dependence on μ suggests a multipole expansion of the correlations by means of Legendre polynomials, $P_l(\mu)$ ³, Coefficients of the expansion can be computed easily in the separations $y/r \ll 1$, i.e. the distant observer limit (DOL), where $\nu \approx 1$ and $\tilde{\mu} = \mu$. We will consider $\langle \xi_{u\delta}^s \rangle_l = 1/(4\pi) \int d\Omega \xi_{u\delta}^s P_l(\mu) d\mu = 1/2 \int d\mu \xi_{u\delta}^s P_l(\mu)$. Evaluating the integrals gives

$$\langle \xi_{u\delta}^s \rangle_0 = -\frac{2\Psi_{\perp} + 2\Psi_{-}/3}{\tilde{r}} \quad (16)$$

$$\langle \xi_{u\delta}^s \rangle_1 = -\left(\frac{3}{5} + \frac{1}{f}\right) \Psi'_{\perp} - \left(\frac{1}{5} - \frac{1}{3f}\right) \Psi'_{-} \quad (17)$$

$$\langle \xi_{u\delta}^s \rangle_2 = -\frac{4}{15} \frac{\Psi_{-}}{\tilde{r}} \quad (18)$$

$$\langle \xi_{u\delta}^s \rangle_3 = \frac{2}{35} (2\Psi'_{\perp} - \Psi'_{-}), \quad (19)$$

and all higher moments vanish identically. The term $2\xi_{uu}/\tilde{r}$ contributes only to $l=0$ and $l=2$ and does not affect any of the other multipoles. Because of the $1/r$ dependence, this term mainly depends on nearby data.

In figure 1 we plot a few of the relevant moments computed from the relations above for the Λ CDM cosmology with the Planck parameters. The multipoles $l=2$ and 3 are much smaller than the others and we opt not to show them. The $l=0$ moment of ξ_{uu}/\tilde{r} is substantial for $r=50h^{-1}$ Mpc. The multipole $l=1$ of this term vanishes identically only in the DOL. Nonetheless, it remains insignificant even away from this limit, as seen from the blue dotted curve at separations $\gtrsim r$. Redshift space distortions boost the correlations with respect to real space due to large scale motions coherent with the density. This is reflected in the higher amplitude of $\langle \xi_{u\delta}^s \rangle_{l=1}$ (solid black for DOL and solid blue for $r=50h^{-1}$ Mpc) relative to the real space $\langle \xi_{u\delta} \rangle_{l=1}$ (dashed). As we shall see, the difference between the DOL and the $r=50h^{-1}$ Mpc results is insignificant compared to the errors associated with observations. The Kaiser rocket effect resulting from the flux limit nature of galaxy redshift surveys amounts to a term of the form ξ_{uu}/\tilde{r} , which is negligible in the $l=1$ moment of the correlation.

4 THE OBSERVATIONS

4.1 The distance indicator catalog

We use the grouped version of the *cosmicflows-3* catalog (Tully et al. 2016) consisting of groups of galaxies as well as individual galaxies unassociated with groups. The total number of objects in the catalog is 6560 with ~ 6200

³ $P_0 = 1$, $P_1 = \mu$, $P_2 = (3\mu^2 - 1)/2$ and $P_3 = (5\mu^3 - 3\mu)/2$.

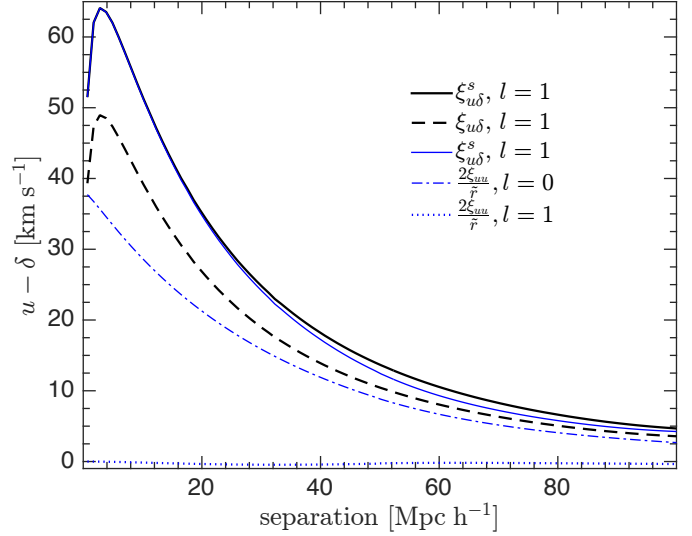


Figure 1. Theoretical multipole moments of various terms in $u - \delta$ correlations, as indicated in the figure. The black solid and dashed curves are, respectively, the redshift and real space dipole ($l=1$) moment of the correlation in the distant observer limit with $r = \infty$. The blue lines are for the case where the u is given at a distance $r = 50h^{-1}$ Mpc from the origin.

having redshifts $cz \lesssim 15000$ km s⁻¹. The catalog provides measurements of redshifts, cz , and distance moduli, $DM = 25 + 5 \log_{10}(D_L/\text{Mpc})$ where D_L is the luminosity distance. To infer the radial peculiar velocities, u , we follow Tully et al. (2016) who use a prescription (Nusser & Davis 1995, 2011; Watkins & Feldman 2014) that avoids introducing spurious non-gaussian errors at large distances.

Uncertainties in the determination of u increase linearly with distance where the error in groups is reduced by the square root of the number of galaxies they respectively contain. Galaxies at large distances are prone to suffer from systematic biases and therefore we choose to restrict our analysis to objects within a maximum redshift of 10000 km s⁻¹, leaving us with ~ 4600 objects.

4.2 The redshift survey

The distribution of galaxies in the flux limited 2MRS catalog (Huchra et al. 2012) will be correlated with peculiar velocities in *cosmicflows-3*. The 2MRS covers most of the sky down to Galactic latitudes of $b \leq 5^\circ$ (8° in the direction of the Bulge) and contains ~ 45000 galaxies with spectroscopic redshifts and with apparent magnitudes $K_s \leq 11.75$. In order to account for the missing galaxies due to the flux limit each galaxy is assigned a weight

$$w = 1/\Phi(r), \quad (20)$$

where $\phi(r)$ is the selection function obtained from the F/T estimator (Turner 1979; Davis & Huchra 1982) taking into account evolution and k-correction (figure 1 in Branchini et al. 2012). The galaxy number density contrast in a small volume, ΔV , is then estimated by

$$\delta^g = \frac{1}{\bar{n}} \sum_{\mathbf{r}_\beta \in \Delta V} w_\beta - 1, \quad (21)$$

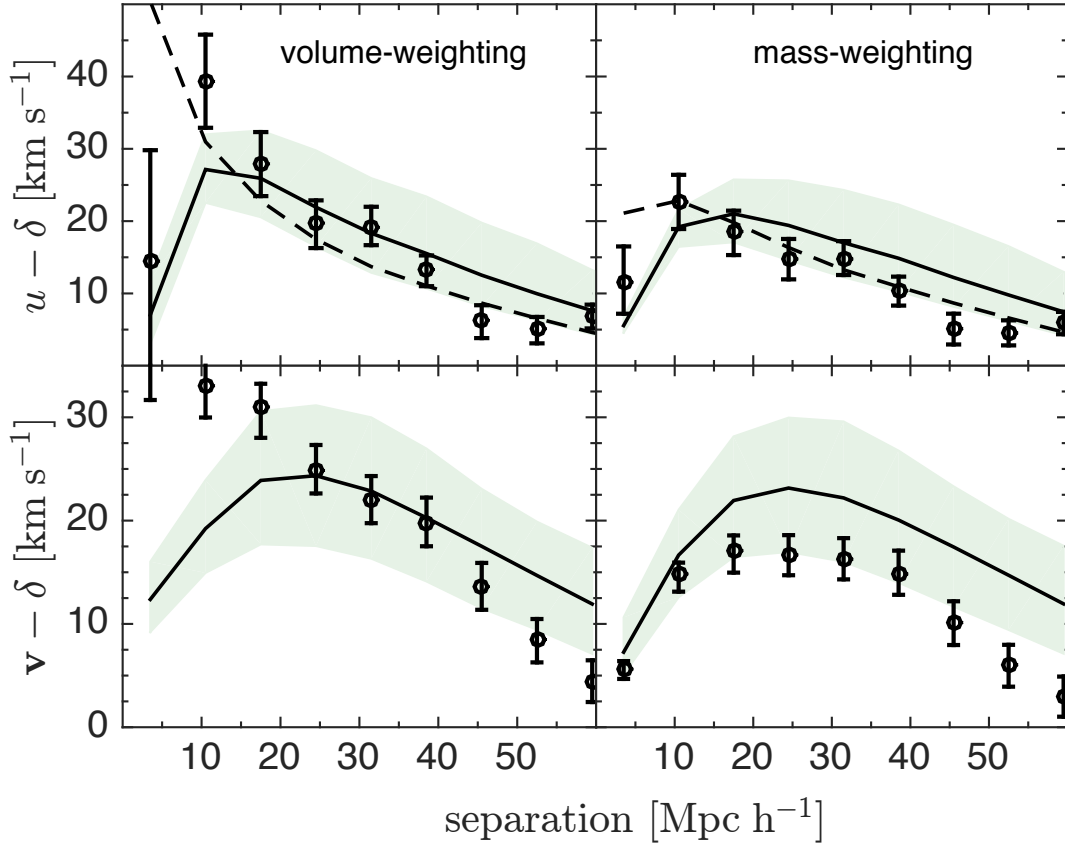


Figure 2. *Top:* Dipole moments, ζ , of the correlations $\xi_{u\delta}^s$ versus the separation, for the data (circles) and the mocks (solid and dashed in redshift and real space, respectively). The (1σ) error bars represent the scatter due random error in *cosmicflows-3* velocities. Colored areas mark 1σ cosmic variance and shot noise in 2MRS, as given from the mocks. Panels to the left and to the right show ζ^V and ζ^M , respectively. *Bottom:* The same as *Top* but for 3D velocities reconstructed using Wiener filtering.

where $w_\beta = w(r_\beta)$ and the sum is over all galaxies in ΔV . Further,

$$\bar{n} = \frac{3}{4\pi R^3} \sum_{r_\beta < R} w_\beta \quad (22)$$

is a proxy to the mean number density of galaxies, computed from the distribution of galaxies out to a sufficiently large radius R . We take $R = 120h^{-1}$ Mpc, but \bar{n} is robust for $80h^{-1}$ Mpc $\lesssim R \lesssim 200h^{-1}$ Mpc, changing by less than a few percents.

4.3 Estimating correlations from the observations

Following the discussion in §3, we consider the dipole ($l = 1$) moment only. We bin the separation, y , into N_b shells with radii y_b ($b = 1 \dots N_b$) of identical widths Δy . For each galaxy, α , at \mathbf{r}_α in the *cosmicflows-3* catalog we compute

$$Q_\alpha = \sum_{y_{\alpha\beta} \approx y_b} w_\beta \mu_{\alpha\beta} \quad (23)$$

where β indicates 2MRS galaxies at \mathbf{r}_β , $\mathbf{y}_{\alpha\beta} = \mathbf{r}_\beta - \mathbf{r}_\alpha$ and $\mu_{\alpha\beta} = \mathbf{y}_{\alpha\beta} \cdot \mathbf{r}_\beta$ is cosine the angle between $\mathbf{y}_{\alpha\beta}$ and \mathbf{r}_β . The approximate symbol in the expression above implies that the summation is over galaxies with $|y_{\alpha\beta} - y_b| < \Delta y$. We

consider two quantities,

$$\zeta^V(y_b) = \frac{1}{N^V} \sum_{\alpha} \frac{Q_\alpha}{\bar{n}V_b} u_\alpha \quad (24)$$

and

$$\zeta^M(y_b) = \frac{1}{N^V} \sum_{\alpha} \frac{Q_\alpha}{\bar{n}V_b(1 + \delta_b^g)} u_\alpha \quad (25)$$

where N^V is the number of objects in the velocity catalog, $\bar{n}V_b$ is the mean number of galaxies in the volume V_b occupied by the corresponding shell, and δ_b is the mean density contrast inside V_b . Both of these quantities reflect the dipole moment of $\xi_{u\delta}^s$, but they have different physical meanings. While ζ^V correlates $u(\mathbf{r})$ with the dipole moment of the density in spherical shell centered on \mathbf{r} , the function ζ^M correlates u with the mean μ per unit mass in the shell, i.e. it gives the same weighting to shells of different densities, δ_b^g . The function ζ^V matches the basic definition of the $l = 1$ multipole of the $u - \delta$ correlation, while ζ^M significantly deviates from it in the non-linear regime where $|\delta_b| \sim 1$. Nonetheless, ζ^M should serve as important test for the robustness of the results.

Let us explore these correlations in more detail. In the

continuous limit

$$\begin{aligned} Q_\alpha(y) &\rightarrow \frac{\bar{n}V_b}{2} \int_{-1}^{+1} [1 + \delta^g(\mathbf{r}_\alpha + \mathbf{y})] \mu d\mu \quad (26) \\ &= \frac{\bar{n}V_b}{2} \int_{-1}^{+1} \delta^g(\mathbf{r}_\alpha + \mathbf{y}) \mu d\mu \end{aligned}$$

where now $\mu = \hat{\mathbf{r}}_\alpha \cdot \hat{\mathbf{y}}$ and $\delta^g(\mathbf{r}_\alpha + \mathbf{y})$ is the density contrast of the 2MRS galaxy distribution at the point $\mathbf{r}_\alpha + \mathbf{y}$ in the shell. Hence,

$$\zeta^V(y) \rightarrow \frac{1}{2N^v} \int_{V^v} d^3\mathbf{r} n^v(\mathbf{r}) u(\mathbf{r}) \int_{-1}^{+1} \delta^g(\mathbf{r} + \mathbf{y}) \mu d\mu, \quad (27)$$

where V^v is the total volume encompassing the peculiar velocity catalog and $n^v(\mathbf{r})$ is the local number density of objects in the catalog, expressed as

$$n^v(\mathbf{r}) = \bar{n}^v [1 + \delta^v(\mathbf{r})] S^v(\mathbf{r}), \quad (28)$$

where \bar{n}^v is the underlying mean number density of objects and δ^v is the underlying density contrast. Clearly δ^v and δ^g are closely related since they represent the underlying distribution of galaxies, albeit of different populations. The function $S^v(\mathbf{r})$ represents various observational selections imposed on objects included in the velocity catalog. In contrast to flux limited redshift surveys, selection criteria on distance measurements are diverse and in general cannot be represented in a well defined form. However, it is reasonable to assume that none of these criteria depend on δ^v . Hence, S^v is independent of δ^v and

$$N^v = \bar{n}^v \int d^3\mathbf{r} S(\mathbf{r}). \quad (29)$$

Taking the ensemble average of the expression (27) we obtain

$$\begin{aligned} \zeta^V &\rightarrow \frac{\bar{n}^v}{N^v} \int d^3\mathbf{r} S(\mathbf{r}) \zeta(r, y) \quad (30) \\ &+ \frac{\bar{n}^v}{2N^v} \int d^3\mathbf{r} S(\mathbf{r}) \langle \delta^v(\mathbf{r}) \delta^g(\mathbf{r} + \mathbf{y}) u(\mathbf{r}) \rangle \mu d\mu. \end{aligned}$$

The second term reflects a high order correlation between the density and velocity fields. We do not focus on this term although it is included in the correlations computed from the mocks used for comparison with data. This term is small on large scales. In the first term

$$\zeta(r, y) \equiv \frac{1}{2} \int \xi_{u\delta}^s(\mathbf{r}, \mathbf{y}) \mu d\mu. \quad (31)$$

Thus the first term is an average of the dipole moment of the underlying linear correlation. Since ζ is independent of the direction of \mathbf{r} , this term is expressed as

$$\frac{4\pi\bar{n}^v}{N^v} \int dr r^2 \bar{S}(r) \zeta(r, y), \quad (32)$$

where \bar{S} is the angular average of $S(\mathbf{r})$, which is simply proportional to the radial distribution of objects in the velocity catalog and it is easily modeled. Further, in the distant observer limit $\zeta(r, y) \approx \zeta(y)$ and we have $\zeta^V \rightarrow \zeta$. To linear order $\zeta^M = \zeta^V$ despite the different physical meanings they carry. On small scales where deviations from linear theory are seen, we expect a smaller amplitude for ζ^M as a result of weighting by the density.

In principle we could assign each *cosmicflows-3* galaxy in this sum a weight determined by the observational error⁴,

⁴ Observational errors include intrinsic scatter in the distance indicator as well as purely instrumental measurement errors

σ^v , in u_α . Since the errors increase linearly with redshift, this procedure will heavily weigh nearer objects. The mean redshift of the *cosmicflows-3* objects (survey depth)

$$\bar{cz} = \sum_{cz_\alpha < cz_{\max}} w_\alpha^v cz_\alpha / \sum w_\alpha^v \quad (33)$$

is $\sim 1000 \text{ km s}^{-1}$ and 5000 km s^{-1} , respectively, for $w^v = (\sigma^v)^{-2}$ and $w^v = (\sigma^v)^{-1}$, both for unrestricted cz_{\max} . Results in this paper will be given with $w = 1$ including objects with within $cz_{\max} = 10000 \text{ km s}^{-1}$, corresponding $\bar{cz} = 8000 \text{ km s}^{-1}$. This equal weighting of all galaxies within cz_{\max} comes at the expense of increased statistical error on the estimated correlations. Fortunately, as we shall see, the main source of uncertainty in the determination of the correlation is cosmic variance rather than velocity observational errors. The reason for imposing the redshift cut, cz_{\max} is to avoid potential systematic errors in the data, which are more likely at larger distances.

We place objects (galaxies and groups) in the peculiar velocity catalog at their comoving distance positions, $r(z)$, computed from observed redshifts, cz , rather than distances, r_e , estimated from the distance indicator measurements. Although the inferred peculiar velocities, u , are the same, the placement of objects at r_e introduces severe spatial Malmquist biases associated with large random errors (Lynden-Bell et al. 1988; Strauss & Willick 1995). Non-linear and incoherent motions on small scales spoil the one-to-one mapping between distance and redshift and play the role of random errors when objects are placed at their redshift coordinates. Thus Malmquist biases are present in redshift space as well. These small scale motions are $\sim 200 \text{ km s}^{-1}$ while distance errors are $\sim (0.15 - 0.2)cz$. Thus, working in redshift space, especially at large distances greatly mitigates the effects of Malmquist biases limiting them to scales of a few Mpc anyways. We will be interested in the correlation signal on scales of 10s of Mpcs, implying that the effect of small scale motions is entirely negligible. Note that the 2MRS galaxy distribution is smeared out along the line of sight due to these motions. This prevents the recovery of the underlying signal on a few Mpc scale even with perfect peculiar velocity data.

A peculiarity of our local cosmological neighborhood is the remarkable coherence of the flow of galaxies within a few Mpcs around us (e.g. Tully et al. 2013). With respect to the CMB frame of reference, the bulk flow around us starts with $\sim 630 \text{ km s}^{-1}$ for the LG and smoothly reaches $\sim 270 \text{ km s}^{-1}$ in a sphere of radius $100h^{-1} \text{ Mpc}$ centered on the observer (Nusser & Davis 2011). Thus, the distribution of galaxies defined by redshifts with respect to the CMB exhibits a large spurious local inhomogeneity. To avoid this behavior we work with redshifts transformed to the LG frame of reference. However, a coherent galaxy distribution is not the only reason for choosing this frame of reference. The LG motion is generated by the cumulative gravitational of the large scale structure out to $\gtrsim 300h^{-1} \text{ Mpc}$ (Blicki et al. 2011; Nusser et al. 2014) and beyond. These distant (external) structures contribute also to the velocities of *cosmicflows-3* objects with respect to the CMB, as indicated by the value of bulk flow within $cz_{\max}/H_0 = 100h^{-1} \text{ Mpc}$. The main contribution of external structures is to the dipole moments of the velocity field on shells around us. However, the dipole component of the velocity field *relative to the LG motion*

is entirely determined by the mass distribution between the LG and the shell (Nusser & Davis 1994). Therefore, working in the LG frame will exclude a velocity component which is uncorrelated with the density field surrounding an object in the *cosmicflows-3* catalog.

5 MOCK CATALOGS

We use 30 mock catalogs of 2MRS extracted by Keselman & Nusser (2016) from the Dark-Sky public Simulations (Skillman et al. 2014) of the Λ CDM cosmology with $\Omega = 0.295$, baryonic density parameter $\Omega_b = 0.0468$, $\Lambda = 0.705$, $h = 0.688$, and *rms* mass density fluctuations in spheres of $8h^{-1}$ Mpc of $\sigma_8 = 0.835$. The parameters are very close to the Planck values (e.g. column 4 of Table 3 in Planck Collaboration et al. 2016). These are dark matter only simulations, but baryonic feedback is too weak to play any significant role over the relevant level of accuracy and scales considered (Hellwing et al. 2016). The simulations are available with 5 different resolutions. The mocks are based on the simulation of 4096^3 particles in a periodic box of $800h^{-1}$ Mpc on the side, corresponding to a particle mass of $6.1 \times 10^8 h^{-1} M_\odot$. We consider halos containing no less than 50 particles, giving a minimal halo mass of $3.05 \times 10^{10} h^{-1} M_\odot$.

Mock ‘‘observers’’ are selected to reside in host halos of mass $\gtrsim 5 \times 10^{11} h^{-1} M_\odot$ corresponding to a Milky Way halo mass with no neighboring rich clusters ($\gtrsim 10^{15} h^{-1} M_\odot$) within a distance of $20 h^{-1}$ Mpc. Further, the bulk velocity within spheres of radii 3, 5, and $7 h^{-1}$ Mpc centered on the observers do not differ by more than 50 km s^{-1} .

Halos above a mass threshold M_h are identified as mock galaxies. The mass threshold depends on the distance from the observer in each catalog in order to match the selection function of the 2MRS galaxies (Branchini et al. 2012). Each catalog is trimmed at a maximum distance of $200h^{-1}$ Mpc and contains ~ 42000 galaxies similar to the real 2MRS.

Similarly to σ_8 for the underlying mass density field, we define σ_8^g as the *rms* of the fluctuations in the galaxy number density contrast in spheres of $8h^{-1}$ Mpc in radius. We also define $b = \sigma_8^g / \sigma_8$ as the galaxy bias factor. Direct calculation of σ_8^g in the mocks in real space yields $b^{\text{mock}} \approx 0.96$, i.e. the mock galaxies are slightly anti-biased. We have directly calculated σ_8^g in the 2MRS catalog from randomly placed spheres. The result depends slightly on the volume chosen to contain the spheres. We obtain $0.98 < \sigma_8^g < 1.07$ for spherical volumes of radii $80 - 140h^{-1}$ Mpc. Thus, we adopt $\sigma_8^g = 1.02 \pm 0.05$ (cf. Westover 2007). We are interested in σ_8^g computed from the galaxy distribution in real space. Assuming the ratio of σ_8^g in redshift to real space is the same as in the mocks we derive $\sigma_8^g = 0.93 \pm 0.05$ for 2MRS in real space. Adopting the Planck $\sigma_8 = 0.831$ (Planck Collaboration et al. 2016) for σ_8 of underlying mass, yields the 2MRS bias factor of $b^{2\text{MRS}} = 1.12 \pm 0.06$.

Mock *cosmicflows-3* galaxies are selected at random the 2MRS mocks with a distance dependent probability designed to produce a radial distribution of objects, consistent with the *cosmicflows-3* catalog. The mean number of galaxies in the mocks within $100h^{-1}$ Mpc is 4300, similar to the observations. We refrain from adding errors to the mock *cosmicflows-3* objects since the observed errors vary depending on the type of distance indicator used and whether the

object is a group or a individual galaxy. The effect of random errors on the correlations is done via a ‘‘bootstrap’’ procedure described in the next section.

6 RESULTS

6.1 $u - \delta$ correlations

The top panels in figure 2 show the correlations ζ computed from the data and the mocks as a function of separation in bins of $7h^{-1}$ Mpc in width. The data correlations are represented by the circles and the attached error bars correspond to the expected *rms* scatter due to random observational errors on peculiar velocities of individual *cosmicflows-3* objects. In order to obtain the error bars, we have perturbed the peculiar velocity of every object in *cosmicflows-3* by a random variable drawn from a normal distribution with *rms* equal to the 1σ velocity error on that object. We have generated a 100 of these bootstrap realizations of the data and computed the corresponding correlation functions. The error bars in the figure are *rms* values of scatter of these correlations from the mean. Thus these error bars do not include cosmic variance and Poisson noise (shot noise) in the 2MRS discrete galaxy distribution. The modeling of these two effects is done via the mock catalogs. The mean correlation functions from the 30 mocks are shown as the solid and dashed curves for redshift and real space, respectively. The light colored shaded areas are the *rms* scatter around the solid curve computed from the 30 mocks in redshift space. Thus the shaded areas include cosmic variance as well as shot noise (but without observational errors on u).

At scales $\lesssim 15h^{-1}$ Mpc, the volume-weighted correlation ζ^V (panel to the left) is larger than ζ^M (panel to the right) in the mass weighting scheme. However, on larger scales, the match between the two functions is good. The data points for both ζ^V and ζ^M match well the corresponding correlations in the mocks. Comparison between the mock correlations in real and redshift space, indicates that the decline of the correlations below separations $\lesssim 15h^{-1}$ Mpc is mostly caused by the smearing out of structure in redshift space as a result of nonlinear and incoherent motions on small scales. On larger scales, the mock correlations are stronger in redshift space than in real space, as expected from the enhanced apparent large scale clustering in redshift space due to coherent motions. On scales $\gtrsim 20h^{-1}$ Mpc, there is a good agreement between the data and the mock on one hand and the theoretical correlations in figure 1 on the other hand. This is reasonable since linear theory is expected to be valid on these scales and the galaxy bias factor in the mocks and the 2MRS is $b \sim 1$.

The total error covariance in the estimation of the correlation functions is obtained by adding the covariance matrices from the mocks and the bootstrap realizations. Using the covariance matrix, C_i , for the 9 measurement points in each of the top panel of figure (2) we compute

$$\chi^2 = \zeta_i C_{ij}^{-1} \zeta_j, \quad (34)$$

where ζ_i is the data correlation. This χ^2 determines whether the *null* hypothesis of *zero* underlying correlation can be ruled out or not within a certain significance level. We find $\chi^2 = 38.67$ and 34.85 for ζ^V and ζ^M , respectively. For 9 degrees of freedom (dof), the χ^2 distribution function yields

a rejection of better than 1.32×10^{-5} and 6.32×10^{-5} for ζ^V and ζ^M , respectively. Expressed in terms of a normal distribution of a single variable, these rejection levels, respectively, correspond to 4.35σ and 4σ . The agreement with the predictions of the Λ CDM model as given by the mocks can similarly be assessed by the same form χ^2 computed with $\zeta - \zeta_{\Lambda\text{CDM}}$ instead of ζ . Here $\zeta_{\Lambda\text{CDM}}$ is the mean of the mock correlations, represented by the solid curves in the figure. We obtain $\chi^2 = 14.97$ and 11.13 for volume and mass weighting, respectively. These values correspond to 1.68σ and 1.11σ levels, making the Λ CDM entirely consistent with the correlation measurements.

6.2 Constraints on the growth rate and clustering amplitude

Predictions of $u - \delta$ correlations from a cosmological model depend on all cosmological parameters. We have seen that the correlation is consistent with the Λ CDM model with the Planck cosmological parameters (Planck Collaboration et al. 2016). Here we aim at deriving constraints on the normalization of the density fluctuations, σ_8 and the growth rate, f , assuming the Planck values for all other cosmological parameters.

The linear theory relation (1) between the velocity and the mass density, implies the scaling $u \propto f\sigma_8$ of the amplitude of u on the combination $f\sigma_8$. From this scaling and the expression (6) it is easy to derive the dependence of $\xi_{u\delta}^s$ on these parameters. The correlation $\xi_{u\delta}^s$ involves the galaxy number density contrast with $\sigma_8^g = b\sigma_8$, hence, in (6) $\xi_{u\delta} \propto bf\sigma_8^2 = f\sigma_8\sigma_8^g$ and $\xi_{uw} \propto (f\sigma_8)^2$. Therefore,

$$\xi_{u\delta}^s = f\sigma_8\sigma_8^g\xi_{u\delta}^1 + (f\sigma_8)^2\xi_{uw}^1 \quad (35)$$

where the superscript ‘‘1’’ indicates correlations computed for $f\sigma_8 = 1$ and we have omitted the ξ_{uu} term which does not contribute to the dipole moment. The correlations $\xi_{u\delta}^1$ and ξ_{uw}^1 could easily be estimated either from the theoretical expressions in §3 or the mock catalogs. Here we work with the mocks since they provide a more realistic description of the data. We extract $f\sigma_8$ by minimizing the function

$$-2\ln P = (\zeta_i - \zeta_i^m)(C^m)_{ij}^{-1}(\zeta_j - \zeta_j^m) + \ln[\det(C^m)] \quad (36)$$

where $\zeta^m(f\sigma_8)$ is the model prediction obtained according to (35) using $\xi_{u\delta}^1$ and ξ_{uw}^1 of the mocks. The covariance matrix C^m depends on $f\sigma_8$ through the cosmic variance term which is also extracted from the mocks assuming it has the same $f\sigma$ scaling as the correlations. Since we are using linear theory to model the dependence on $f\sigma_8$, we limit the calculation of χ^2 in (36) to large scales, including only the 7 points with separations larger than $15h^{-1}$ Mpc. Further, we take $\sigma_8^g \approx 0.93 \pm 0.05$ (cf. §5) in (35). Figure 3 plots curves of $-2\Delta\ln P = -2\ln P + 2\ln[\max(P)]$ for the volume and mass weighting schemes, as indicated in the figure. Minima of $-2\Delta\ln P$ are rendered at the best fit values of $f\sigma_8$ and $-2\Delta\ln P = 1$ mark the corresponding 1σ errors. We find

$$f\sigma_8 = \begin{cases} 0.40 \pm 0.08 & \text{for } \zeta^V \\ 0.32 \pm 0.07 & \text{for } \zeta^M \end{cases} \quad (37)$$

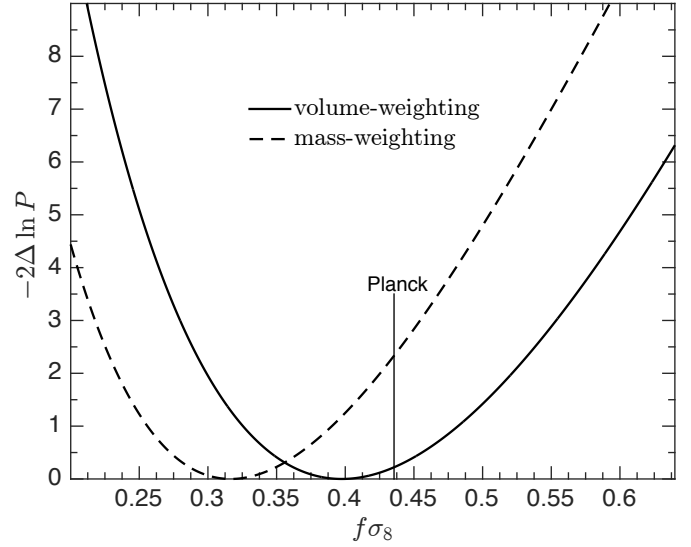


Figure 3. Curves of $-2\Delta\ln P$ (equation 36) versus $f\sigma_8$ derived from the observed ζ^V (solid) and ζ^M (dashed).

which are both consistent with the Planck value $f\sigma_8 = 0.43$. These estimates can be expressed in terms of $\beta \equiv f/b = f\sigma_8/\sigma_8^g$. For $\sigma_8^g = 0.93 \pm 0.05$ we obtain,

$$\beta = \begin{cases} 0.43 \pm 0.09 & \text{for } \zeta^V \\ 0.34 \pm 0.08 & \text{for } \zeta^M \end{cases} \quad (38)$$

The parameters obtained from the two curves are consistent at the $\sim 1\sigma$ level. It is tempting to derive parameters based on the joint measurements of ζ^V and ζ^M . Unfortunately, the number of mocks we have do not allow a robust estimation of the strong covariance between ζ^V and ζ^M . Attempts to do that with the current mocks, lead to a singular covariance matrix.

6.3 $v - \delta$ correlations: preliminary assessment

The 3D velocity is better correlated with the surrounding density fluctuations. This is mathematically evident by the expressions for $\xi_{v\delta}$ and $\xi_{u\delta}$ in §3. Figure 4 illustrates this point. The solid and dashed curves are the dipole moments of the $v - \delta$ correlation from mocks, respectively, for volume and mass weighting schemes. The shaded areas are the corresponding cosmic variance and shot noise scatter. The curves are obtained in a similar way to the calculation of ζ for $u - \delta$, as described in §4.3, with two differences: μ_β is replaced with $\hat{\mathbf{y}} \cdot \mathbf{v}_\alpha / v_\alpha$ in (23) and u_α is replaced with v_α in both (24) and (25). Comparison with the $u - \delta$ correlations in the top panels in figure 2, clearly reveals a stronger $v - \delta$ signal for a similar width of the shaded areas.

The data provides the radial velocities and we need a method for inferring the underlying 3D velocity from sparse and noisy-data. Under the assumption of potential flow (Bertschinger & Dekel 1989), the 3D velocity field can be reconstructed from the observed radial peculiar motions. Observational errors and incomplete spatial coverage in velocity catalogs limit the inference of the 3D flow to large scales only. We employ the methodology of Wiener filter-

ing (Zaroubi et al. 1995) to reconstruct the 3D velocities. Given a set of measurements d_i at points \mathbf{r}_i ($i = 1 \dots N$) the Wiener filtered (WF) field of a desired signal, $F^{\text{WF}}(\mathbf{r})$ at any point \mathbf{r} is

$$F^{\text{WF}}(\mathbf{r}) = \Xi_{r\alpha'} \mathcal{D}_{\alpha\alpha'}^{-1} d_\alpha \quad (39)$$

where Ξ and \mathcal{D} are the “data-data” and “data-signal” correlation matrices. For gaussian errors and a gaussian underlying signal, the field F^{WF} renders a maximum in the probability $P(F|data)$ for F given the data. In our case, F is the 3D velocity field, \mathbf{v} , and d represents the observed radial velocities u . Therefore, $\Xi = \xi_{u\mathbf{v}}$ and $\mathcal{D} = \xi_{uu} + \mathcal{N}$ where \mathcal{N} is the (diagonal) error matrix of u in *cosmicflows-3*. The calculation of these matrices is done using the expressions derived in §3, modified for velocities in the LG frame. Thus instead of $\xi_{uu} = \langle u(\mathbf{r})u(\tilde{\mathbf{r}}) \rangle$ we consider $\langle (u(\mathbf{r}) - \mathbf{v}(0) \cdot \hat{\mathbf{r}})(u(\tilde{\mathbf{r}}) - \mathbf{v}(0) \cdot \hat{\tilde{\mathbf{r}}}) \rangle$ and similarly for $\xi_{u\mathbf{v}}$. In addition to \mathbf{v} , we also apply the WF methodology to derive the most probable real space density contrast field, δ , given the *cosmicflows-3* data. This is done by taking $\Xi = \xi_{u\delta}$ where the $u - \delta$ correlation is given in (13).

The WF 3D velocity, \mathbf{v}^{WF} and the corresponding density contrast, $\delta^{\text{WF}} = -\nabla \cdot \mathbf{v}/f$ on a uniform grid in the supergalactic plane (SGP) are shown in the bottom panel figure 5. The mean velocity in the SGP has been subtracted in order to emphasize the flow pattern in the plane. A comparison the WF reconstruction of Hoffman et al. (2015) for the *cosmicflows-2* (Tully et al. 2013) catalog reveals a good general match. The Perseus-Pisces is apparent as an extended over-density in the bottom-right corner, Coma at the top, a horizontally elongated over-density from $SGX = 0$ to $SGX = -80h^{-1}$ Mpc at $SGY \approx 0$ and a large void in the bottom left corner. The top panel shows contours of $\ln(1+\delta)$ obtained by smoothing the 2MRS galaxy distribution. There is a reasonable visual match between the δ^{WF} and the 2MRS density. While a constant smoothing is applied to the 2MRS, the WF filtering is a strong function of the errors and sparseness of the data. The agreement is satisfactory in light of the error map in figures 6&7. It is interesting that the errors in velocity increase with distance while decrease in the density.

Using \mathbf{v}^{WF} , we compute the dipole moment of the velocity density correlation. Volume and mass weighted dipole moments of $\mathbf{v}^{\text{WF}} - \delta$ are shown in the bottom panels of figure 2. The amplitude of the correlations, both in the data and the mocks, is substantially lower than the amplitude of the unfiltered $\mathbf{v} - \delta$ correlations of in figure 4. The shaded areas representing shot-noise and cosmic variances corresponding to the $\mathbf{v} - \delta$ correlation and shown in the bottom panels of Figure 2 are broader than in the top panels for the $u - \delta$. This may seem surprising since a stronger correlation is expected for the 3D velocity. The reason for that is that the derivation of the 3D velocity is associated with an interpolation of the radial velocity data to all spaces. This effectively introduces additional source of error, as also seen in figures 6&7.

At separations $\gtrsim 15h^{-1}$ Mpc, the data and the mock correlations are in very good agreement for the volume-weighted correlation (left panel). The overall data correlation is below the mock curve in the mass weighting scheme (right panel). However, there is an important caveat in this comparison between data and mocks. The WF introduces a specific form of smoothing which depends on the specific

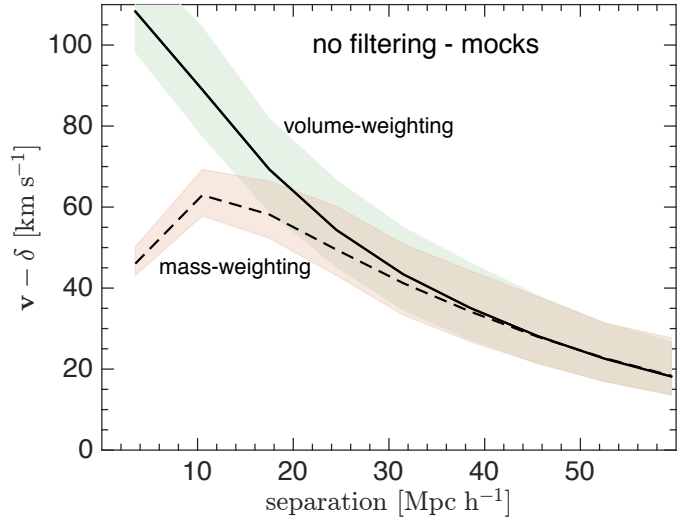


Figure 4. Dipole ($l = 1$) moments of $\mathbf{v} - \delta$ correlations derived from unfiltered peculiar velocities in the mocks.

spatial distribution of data points. To achieve an equivalent smoothing in the mocks, the *cosmicflows-3* data points are padded in each mock and assigned the radial peculiar velocities of the nearest respective mock galaxies. Gaussian random scatter is then added according to the error estimate in the *cosmicflows-3*. This padding of data points in the mocks is done only for the purpose of $\mathbf{v} - \delta$ correlation. It ensures identical WF window for mocks as in data but misses the correspondence between the selection of galaxies in the *cosmicflows-3* and the underlying mass density. More galaxies should be selected in regions of higher density where the flow is convergent, and vice versa. Thus the comparison presented here should only serve as a “proof of concept” motivating a more thorough analysis. A potentially fruitful path to proceed is to augment the \mathbf{v}^{WF} with the missing small scale power according to Hoffman & Ribak (1991). For Gaussian fields, this will yield the most likely unfiltered estimates of the 3D velocities, given the radial peculiar velocities.

7 SUMMARY AND DISCUSSION

Distance measurements are very challenging and the *cosmicflows-3* catalog is under constant “quality control” by its observers. Ongoing improvements in the catalog are expected to reduce systematics, especially at large distances. Following private communications with the observers, we opted to limit the analysis to objects within $cz_{\text{max}} = 10000 \text{ km s}^{-1}$. An attempt to compute the correlation including objects at $cz > cz_{\text{max}}$ failed to reach converging results. As seen in figure 2, it is cosmic variance rather than random observational errors that constitute the main source of random uncertainty in $u - \delta$. Suppression of cosmic variance requires a significant increase in the volume probed

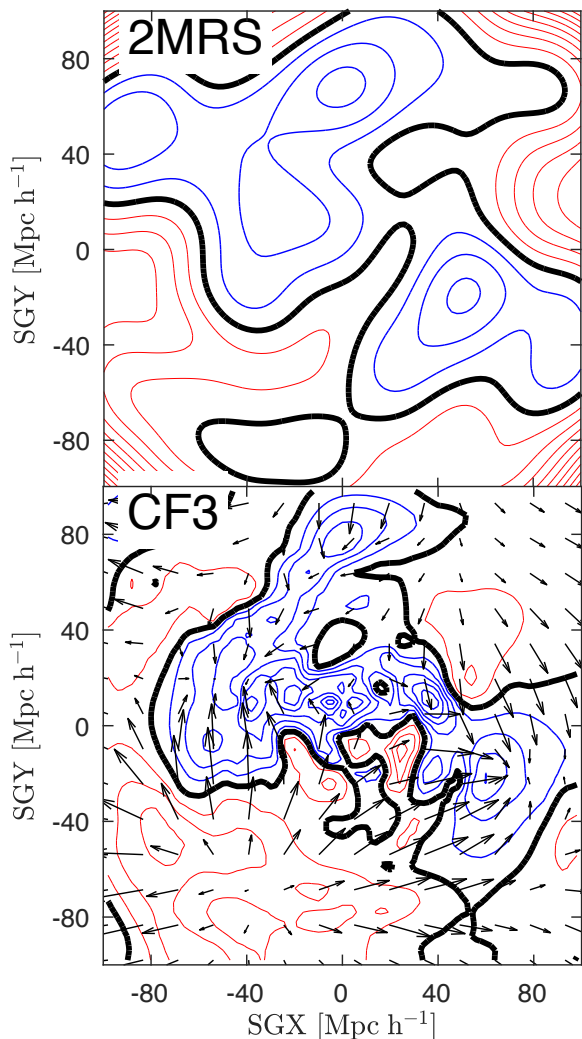


Figure 5. *Top:* Contour map of the natural logarithm of the 2MRS density field smoothed with a Gaussian window of $10h^{-1}$ Mpc in width. *Bottom:* The velocity field \mathbf{v}^{WF} overlaid on maps of $\delta^{\text{WF}} = -\nabla \cdot \mathbf{v}^{\text{WF}}/f$, obtained by Wiener filtering of *cosmicflows-3*. Arrow lengths are proportional to the amplitude of the velocity where the arrow nearest to the bottom-left corner corresponds to 360 km s^{-1} . Both panels show fields in the supergalactic plane and the contour spacing is 0.25. Black, blue and red contours correspond to zero, positive and negative density contrast, respectively.

by velocity catalogs. The next *cosmicflows-4* is expected to have a better control of systematics, allowing us to use data at larger distances with greater confidence. Another important likely development is the likely HI SKA precursor telescopes (e.g. Blyth 2015), which could potentially provide Tully-Fisher distances for tens of thousands of galaxies within $300h^{-1}$ Mpc.

It is encouraging that the constraints derived here are consistent with other estimates based on 2MASS galaxies

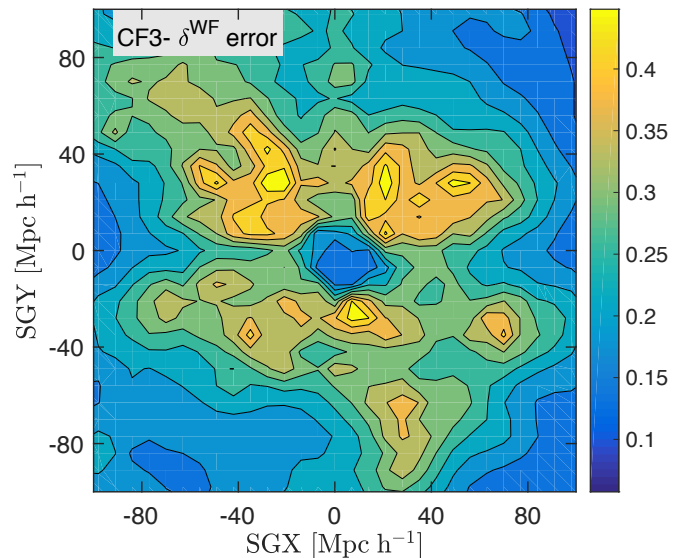


Figure 6. Map of the expected 1σ error in δ^{WF} .

(e.g. Pike & Hudson 2005; Erdogdu et al. 2005; Lavaux et al. 2008; Bilicki et al. 2011; Branchini et al. 2012). In particular, the detailed analysis of Davis et al. (2011) have demonstrated an excellent alignment between the velocity field from the SFI++ catalog of peculiar velocities and the gravitational force field obtained from the $K_s = 11.25$ 2MRS of ~ 2300 galaxies. The alignment is best for $\beta = 0.33 \pm 0.045$ which is in excellent agreement with both $\beta = 0.34 \pm 0.08$ (mass weighting) and $\beta = 0.43 \pm 0.09$ (volume weighting). This is perhaps not surprising since *cosmicflows-3* relies heavily on the SFI++ and the $K_s = 11.75$ 2MRS is selected from the same galaxy population as the $K_s = 11.25$. Still the agreement is impressive given the different methodologies.

Velocity-density correlations play a role in the modeling of redshift distortions in the density auto correlation function as estimated from redshift surveys (Koda et al. 2014; Okumura et al. 2014; Sugiyama et al. 2015). Thus the analysis presented here could be useful since it provides direct observational constraints on these correlations.

Velocity-velocity ($u-u$) correlations can be computed directly from peculiar velocity catalogs. Galaxy motions are unbiased tracers of the underlying velocity field. Thus, in principle, $u-u$ correlations are independent of galaxy bias, unlike $u-\delta$ correlations. However, in practice $u-u$ correlations are affected by the distribution of objects in the velocity catalog. Further, they are prone to larger cosmic variance uncertainties (Hellwing et al. 2017). Therefore, $u-\delta$ correlations may prove more robust and useful.

Peculiar velocities induce spatial modulations of the observed galaxy luminosity function (when redshifts are used to transform fluxes to luminosities). Thus spatial luminosity variations could serve as a probe of peculiar motions (Tammann et al. 1979; Nusser et al. 2011; Feix et al. 2015, 2017). Thus useful information could be extracted by cor-

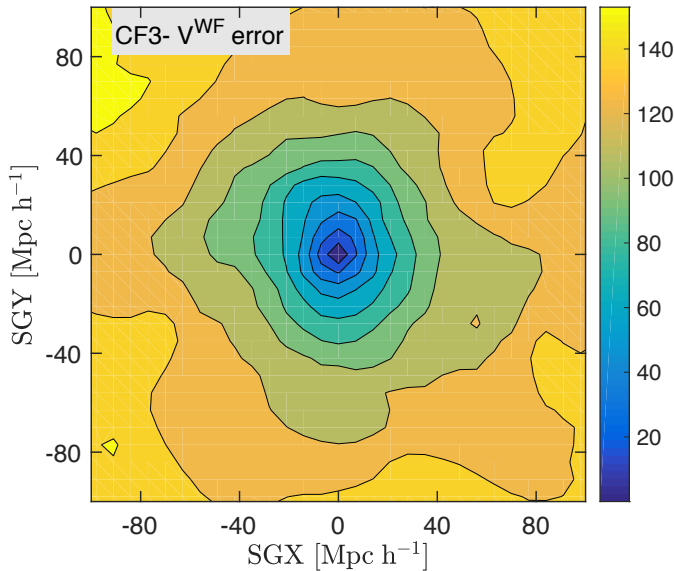


Figure 7. Map of the expected 1σ error (in km s^{-1}) in v^{WF} .

relating spatial deviations from the global luminosity function on one hand and the surrounding galaxy distribution on the other. This particular application of the luminosity modulation method could be susceptible to environmental dependences of the luminosity function. Nevertheless, the application should at least yield upper limits on the amplitude of the correlations.

While this paper is in the production stages, [Adams & Blake \(2017\)](#) presented an analysis of the density-velocity covariance to improve cosmological constraints using 6dF data ([Jones et al. 2004](#)).

ACKNOWLEDGMENTS

The author thanks Enzo Branchini, Marc Davis, Maciek Bilicki and Wojtek Hellwing for useful comments. This research was supported by the I-CORE Program of the Planning and Budgeting Committee, THE ISRAEL SCIENCE FOUNDATION (grants No. 1829/12 and No. 203/09) and the Asher Space Research Institute.

REFERENCES

Adams C., Blake C., 2017, arXiv:1706.05205
 Bertschinger E., Dekel A., 1989, *ApJ*, 336, L5
 Bilicki M., Chodorowski M., Jarrett T., Mamon G., 2011, *ApJ*, 741, 31
 Blyth S. L., 2015, in Proc. Sci. pp 496–499 (arXiv:1109.5605), doi:10.1017/S1743921312009702, <http://arxiv.org/abs/1109.5605><http://dx.doi.org/10.1017/S1743921312009702>
 Branchini E., Davis M., Nusser A., 2012, *MNRAS*, 424, 472
 Carrick J., Turnbull S. J., Lavaux G., Hudson M. J., 2015, *MNRAS*, 450, 317

Ciecielag P., Chodorowski M., 2004, *MNRAS*, 349, 945
 Davis M., Huchra J., 1982, *ApJ*, 254, 437
 Davis M., Nusser A., Masters K. L., Springob C., Huchra J. P., Lemson G., 2011, *MNRAS*, 413, 2906
 Erdogdu P., et al., 2005, *MNRAS*, 368, 1515
 Feix M., Nusser A., Branchini E., 2015, *Phys. Rev. Lett.*, 115, 011301
 Feix M., Branchini E., Nusser A., 2017, *MNRAS*, 467, 468
 Gorski K., 1988, *ApJ*, 332, L7
 Hellwing W. A., Schaller M., Frenk C. S., Theuns T., Schaye J., Bower R. G., Crain R. A., 2016, *MNRAS*, 461, L11
 Hellwing W. A., Nusser A., Feix M., Bilicki M., 2017, *MNRAS*, 467, 2787
 Hoffman Y., Ribak E., 1991, *ApJL*, 380, L5
 Hoffman Y., Courtois H. M., Brent Tully R., 2015, *MNRAS*, 449, 4494
 Huchra J., et al., 2012, *ApJS*, 199, 26
 Jones D. H., et al., 2004, *MNRAS*, 355, 747
 Kaiser N., 1988, *MNRAS*, 231, 149
 Keselman A., Nusser A., 2016, *MNRAS*, 467, 1915
 Koda J., et al., 2014, *MNRAS*, 445, 4267
 Kogut A., et al., 1993, *ApJ*, 419, 1
 Lavaux G., Tully R. B., Mohayaee R., Colombi S., 2008, *ApJ*, 709, 483
 Linder E. V., 2005, *Phys. Rev. D*, 72, 043529
 Lynden-Bell D., Faber S. M., Burstein D., Davies R. L., Dressler A., Terlevich R. J., Wegner G., 1988, *ApJ*, 326, 19
 Lynden-Bell D., Lahav O., Burstein D., 1989, *MNRAS*, 241, 325
 Nusser A., Davis M., 1994, *ApJL*, 421, L1
 Nusser A., Davis M., 1995, *MNRAS*, 276, 1391
 Nusser A., Davis M., 2011, *ApJ*, 736, 93
 Nusser A., Branchini E., Davis M., 2011, *ApJ*, 735
 Nusser A., Davis M., Branchini E., 2014, *ApJ*, 788, 157
 Okumura T., Seljak U., Vlah Z., Desjacques V., 2014, *JCAP*, 2014, 003
 Peebles P. J. E., 1980, *The large-scale structure of the universe*. Princeton University Press, NJ, <http://adsabs.harvard.edu/abs/1980lssu.book.....P>
 Pike R. W., Hudson M. J., 2005, *ApJ*, 635, 11
 Planck Collaboration et al., 2016, *A&A*, 594, A13
 Sachs R., Wolfe A., 1967, *ApJ*, 147, 73
 Schmoldt I., et al., 1999, *MNRAS*, 304, 893
 Skillman S. W., Warren M. S., Turk M. J., Wechsler R. H., Holz D. E., Sutter P. M., 2014, *Arxiv:1407.2600*, p. 26
 Springob C., Masters K., Haynes M., Giovanelli R., Marinoni C., 2007, *apjs*, 172, 599
 Strauss M., Davis M., 1988, in , *Large-Scale Motions Universe A Vatican study Week*. Princeton University Press, NJ, pp 255–274
 Strauss M., Willick J., 1995, *Physics Reports*, 261, 271
 Sugiyama N. S., Okumura T., Spergel D. N., 2015, *JCAP*, 7, 18
 Tammann G., Yahil A., Sandage A., 1979, *ApJ*, 234, 775
 Tully R. B., et al., 2013, *ApJ*, 146, 86
 Tully R. B., Courtois H. M., Sorce J. G., 2016, *Astron. J.*, 152, 1
 Turner E. L., 1979, *Astrophys. J.*, 231, 645
 Watkins R., Feldman H. A., 2014, *MNRAS*, 450, 1868
 Westover M., 2007, PhD thesis, Harvard University
 Zaroubi S., Hoffman Y., Fisher K., Lahav O., 1995, *ApJ*, 449, 446